IEEE Access
Multidisciplinary | Rapid Review | Open Access Journal

Received March 13, 2021, accepted March 25, 2021, date of publication April 9, 2021, date of current version June 24, 2021.

Digital Object Identifier 10.1109/ACCESS.2021.3072146

A Fully Polarized Antenna Covering the Hemispherical Airspace

JIASHAN LIU, HONGDA LU, (Member, IEEE), KE PANG, ZHIPENG LIU, YONG LIU, (Member, IEEE), AND XIN LV, (Member, IEEE)

Beijing Key Laboratory of Millimeter Wave and Terahertz Technology, School of Information and Electronics, Beijing Institute of Technology, Beijing 100081, China

Corresponding author: Yong Liu (fatufo@bit.edu.cn)

This work was supported in part by the National Natural Science Foundation of China under Grant 61901040, and in part by the Major Instrument Project of the National Natural Science Foundation of China under Grant 61527805.

ABSTRACT A fully polarized antenna has been proposed in this paper. The antenna is composed of four independent antennas, named X, Y, H, V. The simulation and measurement results verify the independent antenna radiation performance and the function of the fully polarized antenna. From 2.33 GHz to 2.45 GHz (4.1% impedance bandwidth), the S_{11} parameters of all antennas are lower than -10 dB. The S_{21} parameters tested among antennas are lower than -23.0 dB in the 2.2-2.6 GHz frequency band. The X and Y antenna cover the $0° < \theta < 60°$ airspace and the H and V antenna cover the $60° < \theta < 90°$ airspace. The independent antenna polarization has been accurately present, and the orthogonality of the polarization has been verified. The X and Y antenna cover orthogonal polarized radiation in 93.4% of hemisphere and the H and V antenna cover 87.8%. The not orthogonal area is far away from their main research area. Experiments for the unknown polarization waves analysis and the antenna pattern reconstruction are implemented to demonstrate the polarization coverage and application potential of the fully polarized antenna.

INDEX TERMS Fully polarized antenna, polarization coverage airspace, polarization analysis, pattern reconstruction.

I. INTRODUCTION

Recently, the demand for fully polarized information has gradually increased. The fully polarized information is mainly used in two aspects: The first aspect is expanding the channel capacity of communication applications. It has been pointed out that the tri-polarized communication system could obtain 3 times the theoretical channel capacity [1] and is insensitive to the orientation of the transceiver antenna. A time-varying statistical channel model [2] for a tri-polarized antenna system has been proposed to proves that the correlation between multi-polarized channels is extremely low, and the sensitivity of the communication antenna can be reduced when the transceivers are all fully polarized antennas. The second aspect is to provide different polarization channels for radar applications. The tri-polarized adaptive array can achieve better interference suppression effects [3]. In the sensor array filtering applications, the tri-polarized antenna can obtain better SNR(Signal to Noise Ratio) when the interfering signal is cross-polarized [4].

Almost all proposed fully polarized antennas are tri-polarized antennas, and there are two kinds: The first is the combination of a dual-polarized antenna and a single-polarized antenna. The X-Y polarization usually uses the same resonant mode, such as dual-polarized microstrip antenna [5] and dual-polarized dielectric resonant antenna [6]. Z polarization is implemented by dipole or monopole [7]. The second is the combination of three single-polarized antennas. The basic antennas include dipole antenna [8], slot antenna [9] and loop antenna [10].

The tri-polarized antenna corresponds to the full polarization (three polarization) model used in the theoretical analysis. Although the polarization coverage has been improved to some extent, the full polarization coverage of the airspace is not completely evaluated. It is difficult to achieve full polarization coverage without zeros in the hemispherical airspace due to the platform and feeding structure. For example, the microstrip antenna has low gain in the low latitude direction, while the monopole antenna can only provide vertical

The associate editor coordinating the review of this manuscript and approving it for publication was Sotirios Goudos.

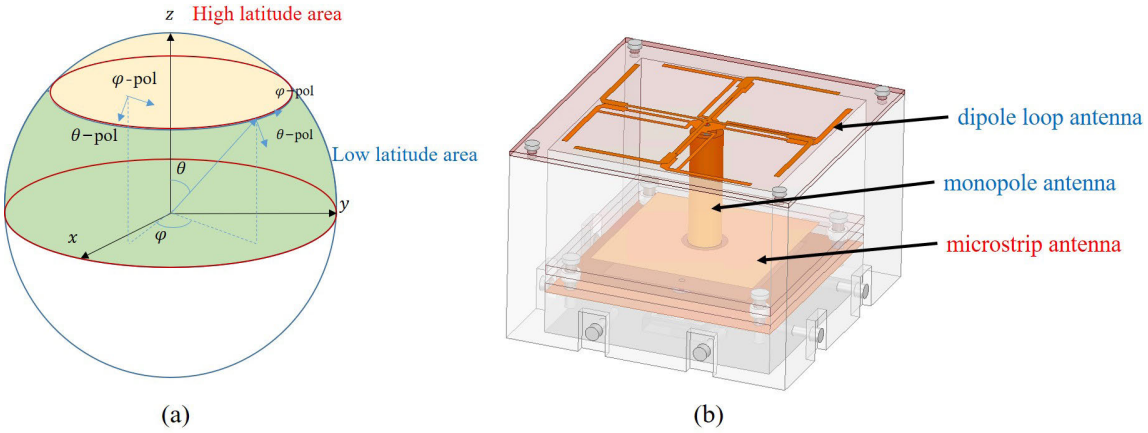

FIGURE 1. Fully polarized antenna design. (a) Hemispherical space division. (b) Fully polarized antenna structure.

polarization gain in the low latitude direction, which is not sufficient to achieve full polarization coverage in the low latitude direction. In the papers concerning the fully polarized antennas, the fully polarized coverage of the hemisphere is hardly mentioned. The fully polarized antenna proposed in this paper radiates the dual-polarization in the hemispherical airspace, by feeding two sets of orthogonal modes for the high latitude area and the low latitude area separately. The fully polarized antenna covering the hemisphere can be widely used in MIMO communication, Full polarization detection arrays, and other applications.

This work is organized as follows: Section II introduces the idea of the proposed fully polarized antenna and design details; Section III presents the port performance and radiation performance of four independent antennas; Section IV introduces the configuration and function of the fully polarized antenna. finally, a short conclusion is given.

II. IDEA AND DESIGN

Full polarization coverage requires that the antenna must have two independent radiation modes with orthogonal polarization in the radiation direction. The hemisphere coverage is meaningful enough for practical antenna. The upper hemisphere can be divided into two areas: low latitude area and high latitude area. Fig.1(a) is a schematic diagram of hemispherical airspace.

A dual-polarized microstrip antenna (the X and Y antenna) is designed to cover the high latitude area. The dual-polarized microstrip antenna can be regarded as a magnetic current binary array, and the two binary arrays with 90° rotation symmetry can achieve full polarization coverage in the high latitude direction. A linear current source and the duality are combined to cover the low latitude area. According to the duality, the amplitude pattern of current and the amplitude pattern of magnetic current have the same shape, only the electric field polarization patterns are orthogonal. A dipole loop antenna (the H antenna) is used to achieve equivalent linear magnetic current radiation. The dipole loop antenna is fed from the center of the fully polarized antenna, which can improve the uniformity of the pattern. A monopole antenna (the V antenna) is used to achieve equivalent current radiation. The copper tube monopole is wrapped around the feedline of the dipole loop antenna to avoid structural interference.

Fig.1(b) shows the structure of the fully polarized antenna. All feeding ports are under a 6 mm aluminum plate. The radiators include a dual-polarized microstrip antenna, a monopole, and a dipole loop antenna. The overall size of the antenna is 62 mm × 62 mm × 42 mm. The detailed size of each antenna is shown in Fig.2. The microstrip antenna adopts the double-layer coupling patches structure to expand bandwidth. The monopole and the feedline of the dipole loop antenna pass through the hole in the center of the patches. The antenna is surrounded by a nylon radome to provide structural stability.

III. INDEPENDENT ANTENNA PERFORMANCE

This section presents the measured performance of the independent antennas in the fully polarized antenna. The port VSWR of the fully polarized antenna is shown in Fig.3(a). The matching performance of the X antenna and the Y antenna are almost the same due to the 90° rotational symmetry. The X antenna working frequency band covers 2.33-2.50 GHz and the relative bandwidth is 7.1%. The working frequency band of the Y antenna covers 2.34-2.51 GHz and the relative bandwidth is 7.1%. The working frequency band of the H antenna covers 2.35-2.54 GHz and the relative bandwidth is 7.9%. The V antenna working frequency band covers 2.36-2.46 GHz and the relative bandwidth is 4.1%. Among the four antennas, the V antenna bandwidth is the smallest. In the range of 2.36 GHz to 2.46 GHz, the S_{11} parameters of all antenna ports are less than −10 dB, and the impedance bandwidth is 4.1%.

Fig.3(b) presents the coupling among the four ports of the fully polarized antenna. The S_{21} parameters tested between each port are less than −23.0 dB in the 2.2-2.6 GHz frequency

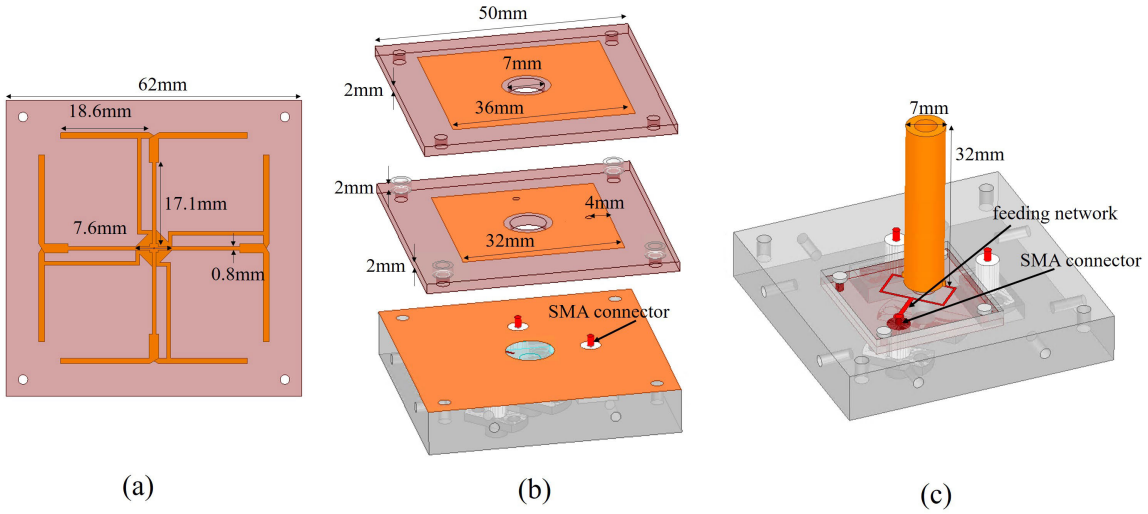

FIGURE 2. The details of each part of the fully polarized antenna. (a) The dipole loop antenna. (b)The dual-polarized microstrip antenna. (c) The monopole antenna.

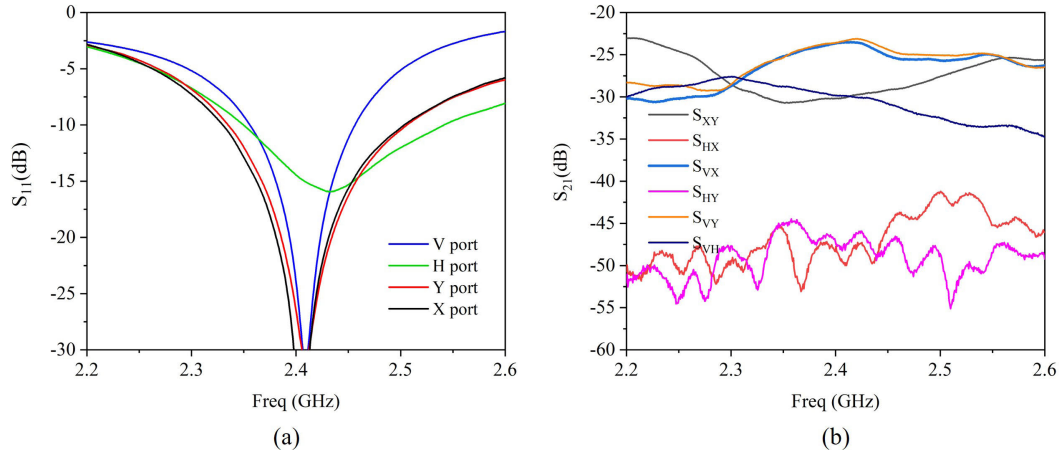

FIGURE 3. Full polarization antenna measured port performance. (a) Port matching performance (S_{11}). (b) Port coupling performance (S_{21}).

band. the coupling between the X port and the Y port is due to the shared structure of the patches, and the coupling is lower than −23.0 dB in 2.2-2.6 GHz. The coupling between the X/Y port and the V port is between −31.0 dB and −23.4 dB. In the area where the radiation range of the V antenna overlaps with the radiation range of the microstrip antenna, the polarization of the V antenna and the polarization of the X/Y antenna are matched. The radiation ranges of the H port and the V port almost overlap, and the coupling between the H port and the V port is between −35.1 dB and −27.5 dB. The coupling performance between the X/Y port and the H port is less than −42.1 dB. The H antenna radiation range overlaps with the X/Y antenna radiation range in a small area. And the H antenna polarization is orthogonal to the X/Y antenna polarization. Overall, the measured data demonstrate that the fully polarized antenna works at the working frequency around 2.4 GHz, and the ports operate independently.

Fig.4 shows the radiation performance of each antenna in the fully polarized antenna. Fig.4 (a-c) presents the X antenna radiation performance. Fig.4 (a) is a heat map of the X antenna radiation pattern in the entire airspace. It can be seen that the radiated energy of the antenna gradually decreases when θ increases. At the $\theta = 90°$ direction, the radiation energy of φ=90° and φ=−90° is greater than φ=0° and φ=180° directions. Fig.4 (b) is a diagram of the co-pol and x-pol of the X antenna E plane and H plane in the range of $-80° < \theta < 80°$. It can be seen that the test data of the co-pol pattern almost matches the simulation data, and the maximum gain is 6.5 dB. The x-pol test data is lower than −20.8 dB. Fig.4 (c) shows the phase distribution on the E plane and H plane in the range of $-80° < \theta < 80°$. The distribution of the X antenna radiation phase pattern is almost uniform. The difference between the maximum value and the minimum value of the co-pol phase on the E plane is 4.3°, and

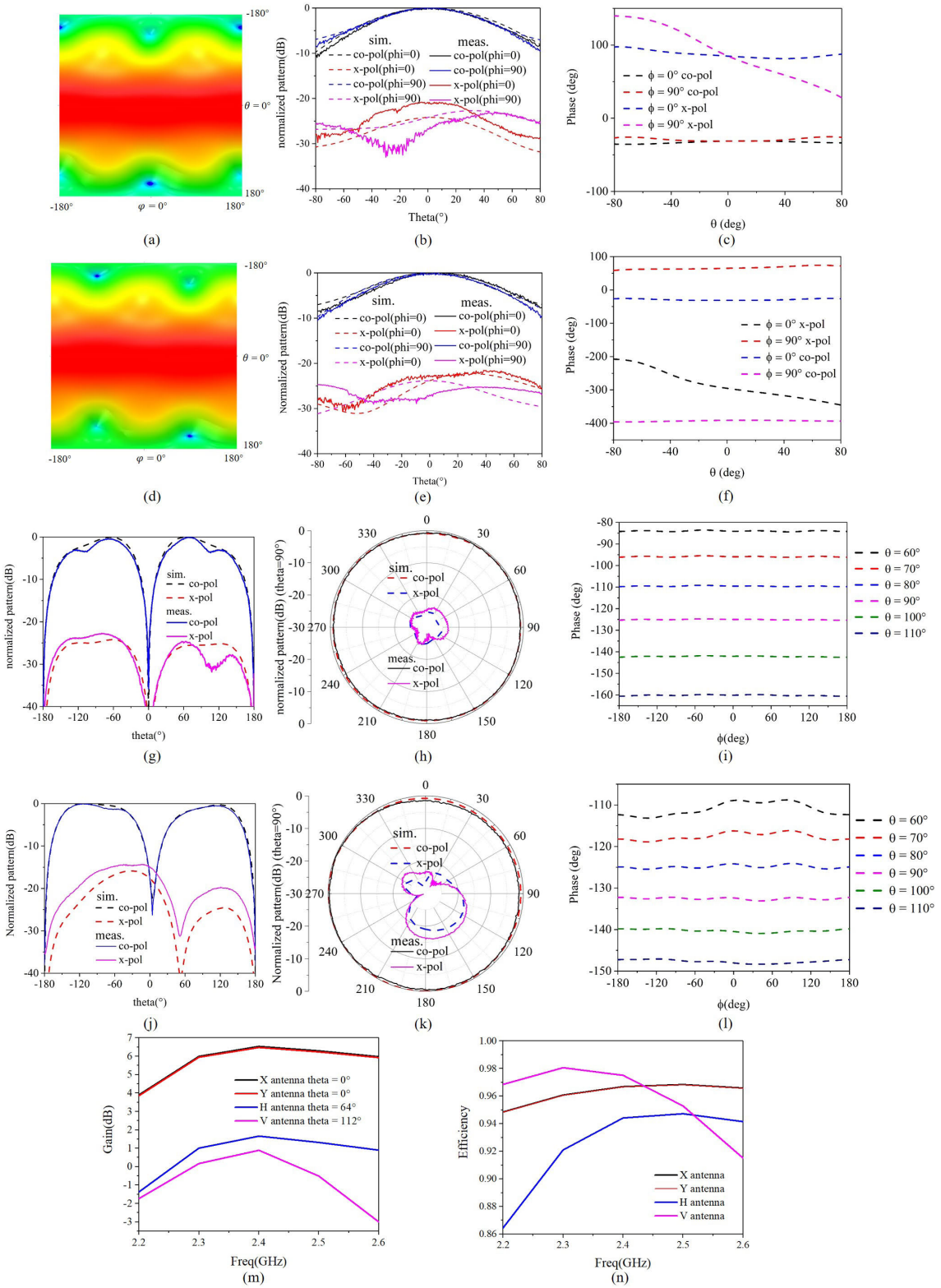

FIGURE 4. Radiation performance of each antenna in the fully polarized antenna. (a) The X antenna radiation heat map. (b) The co-pol and x-pol of the X antenna. (c) The phase pattern of the X antenna. (d) The Y antenna radiation heat map. (e)The co-pol and x-pol of the Y antenna. (f) The phase pattern of the Y antenna. (g) The co-pol and x-pol of the H antenna in H plane. (h) The co-pol and x-pol of the H antenna in E plane. (i) The phase pattern of the H antenna. (j) The co-pol and x-pol of the V antenna in E plane. (k) The co-pol and x-pol of the V antenna in H plane. (l)The phase pattern of the V antenna. (m) The gain of antennas in the fully polarized antenna. (n) The radiation efficiency of antennas in the fully polarized antenna.

the difference between the maximum value and the minimum value of the co-pol phase on the H plane is 5.1°.

Fig.4 (d-f) presents the Y antenna radiation performance. Fig.4 (d) is a heat map of the Y antenna radiation pattern in the entire airspace. At the $\theta = 90°$ direction, the radiation energy of φ=0° and φ=180° is greater than φ=90° and φ=−90° directions. The 90° rotation in φ of Fig.4 (d) is equivalent to 4 (a). Fig.4 (e) is a diagram of the co-pol and x-pol of the Y antenna E plane and H plane in the range of $-80° < \theta < 80°$. It can be seen that the test data of the co-pol pattern almost matches the simulation data, and the maximum gain is 6.5 dB. The x-pol test data is lower than −21.5 dB. Fig.4 (f) shows the phase distribution on the E plane and H plane in the range of $-80° < \theta < 80°$. The distribution of the Y antenna radiation phase pattern is almost uniform. The difference between the maximum value and the minimum value of the co-pol phase on the E plane is 4.4°, and the difference between the maximum value and the minimum value of the co-pol phase on the H plane is 4.9°.

Fig.4 (g-i) presents the H antenna radiation performance. Fig.4 (g) and (h) show the results of co-pol and x-pol in the E plane and H plane. It can be seen that the test data of the co-pol pattern is consistent with the shape of the simulation data. On the $\varphi = 0°$ plane (H plane), the co-pol radiation gain has a depression between 90° and 110°, which may come from the metal platform under the antenna. The maximum gain is 1.7dB, and the x-pol test data is lower than −22.8 dB. the difference between the maximum value and the minimum value of the co-pol gain on the $\varphi = 90°$ plane (E plane) is 0.5 dB. Fig.4 (i) shows the phase distribution of the H antenna when θ is fixed from 60° to 110°. The difference between the maximum phase and the minimum phase is 1.6°, which appears at the θ=60°.

Fig.4 (j-l) presents the V antenna radiation performance. Fig.4 (j) and (k) show the results of co-pol and x-pol in the E plane and H plane. It can be seen that the test data of the co-pol pattern is consistent with the simulation data. The x-pol test data is about 2-3 dB worse than the simulated data, which is lower than −14.3 dB. When $\varphi = 0°$, the maximum gain of co-pol is 0.9 dB. the difference between the maximum value and the minimum value of the co-pol gain on the $\varphi = 90°$ plane (H plane) is 1.0 dB. From the Fig.2 (c), it can be seen that the V port is at the −135° direction of the central axis. Fig.4 (l) shows the phase distribution when θ is fixed from 60° to 110°. the difference between the maximum phase and the minimum phase is 5.2° at θ=60°.

Fig.4 (m) presents the gain of antennas in the fully polarized antenna. The maximum gain of X and Y is at $\theta = 0°$, which is similar to each other. The maximum gain of H is at $\theta = 64°$, which is 1.7 dB. The gain of H decreases rapidly with decreasing frequency. The maximum gain of V is at $\theta = 112°$, which is 0.9 dB. The gain of V decreases rapidly with increasing frequency. Fig.4 (n) presents the simulated radiation efficiency of antennas in the fully polarized antenna. The radiation efficiency of each antenna is better than 0.86.

The radiation polarization of any radiator in the far field can be regarded as an elliptical polarization. This ellipse can be represented by the amplitude and phase values of two orthogonal polarization components:

$$\hat{\theta}A_\theta \cos(\omega t + P_\varphi) + \hat{\varphi}A_\varphi \cos(\omega t + P_\varphi) \quad (1)$$

The amplitude and phase data of the far-field θ and φ polarization components are derived when each antenna is independently fed. The far field data comes from the simulation results of the commercial software package HFSS (High Frequency Structure Simulator). Radiation polarization ellipses of each antenna on the far-field airspace have been calculated.

Firstly, the polarization type has been determined. Fig.5 gives the axial ratio of each antenna on the far field respectively. The sampled distribution diagram of θ angle interval 10° and φ angle interval 10° has been shown in Fig.5. The vertical axis is the θ axis, which increases from 0° to 180°; the horizontal axis is the φ axis, which increases from 0° to 360°. For antennas with different radiation areas, the research area has been framed by a black box. For the X antenna and Y antenna, the framed angle range is $0° < \theta < 60°$. For the H antenna and V antenna, the framed angle range is $60° < \theta < 90°$. It can be seen from Fig.5 that the radiation axis ratio in the selected range is far greater than 10 dB. So it can be determined that the radiation polarization generated by independent antennas is linear in the operating area.

Secondly, the specific direction of the polarization ellipse long axis has been calculated to determine whether the fully polarized antenna can achieve polarization coverage in the hemisphere airspace. Fig.6 presents the polarization direction of each antenna. The sampled distribution diagram of θ angle interval 10° and φ angle interval 10° in Fig.6. The polarization direction in Fig.6 is represented by the angle between the polarization direction and the θ axis. For example, when the polarization direction angle of a certain polarization is 28°, it indicates that the far-field polarization is pointing to the angle that rotates 28° from the θ axis counterclockwise. It can be seen that the polarization distribution of the X antenna or the Y antenna is the 90° rotational transformation in the φ direction of each other. When φ rotates from 0° to 90°, the polarization direction rotates too. Therefore, in the research airspace, the intersection angle of the polarization direction between the X antenna and the Y antenna is 90°. For the H antenna, the polarization direction of the airspace is 90° (φ direction), and for the V antenna, the polarization direction of the airspace is 0° or 180° (θ direction). The intersection angle of the polarization direction between the H antenna and the V antenna is 90°.

In order to accurately illustrate the orthogonality of the antenna polarization, Fig.7 presents the polarization intersection angle for X-Y and H-V. The range of 90°±20° is determined as orthogonal polarization. Because two equal orthogonal E-field compose 3 dB axis ratio circular polarization at 90°±20°. It can be concluded that the angle range of the polarization between the X antenna and Y antenna

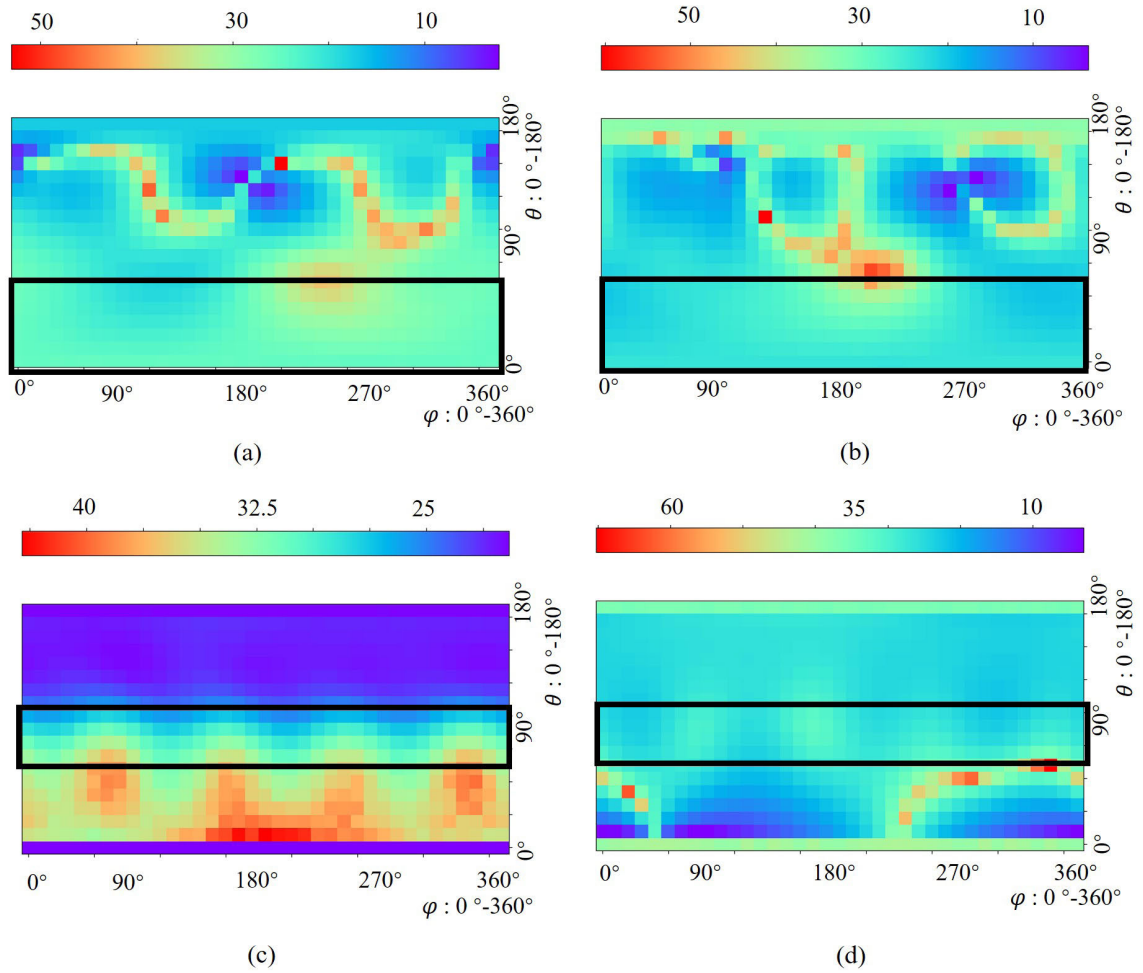

FIGURE 5. The radiation axial ratio of each antenna in the fully polarized antenna. (a) The X antenna. (b) The Y antenna. (c) The H antenna. (d) The V antenna.

that satisfies the orthogonal condition accounts for 93.4% of the whole airspace. And the area that does not satisfy the orthogonal conditions is in the low latitude radiation direction, far away from the research area of the X and Y. The angle range of the polarization between the H and V that satisfies the orthogonal condition accounts for 87.8% of the whole airspace. And the area that does not satisfy the orthogonal conditions is in the high latitude radiation direction, far away from the research area of the H and V. In summary, the polarization can be regarded as orthogonal in the whole hemisphere.

It is assumed that there is a phase center for each independent antenna. The far field expression of the radiation field can be expressed by multiplying the initial electric field vector and the phase [11]:

$$\vec{E}_r = (\hat{\theta}E_\theta(\theta,\varphi) + \hat{\varphi}E_\varphi(\theta,\varphi))e^{-jk\cdot(r-r_0)} \tag{2}$$

In Eq.2, k represents the phase constant in the air, and r_0 is the coordinate position of the phase center. The Eq.2 represents the electric field on the whole airspace. When the studied airspace is limited to the xoz plane, the electric field phase can be simplified as:

$$\psi(\theta) = k \cdot (x_0 \sin\theta + z_0 \cos\theta) + \psi_0 \tag{3}$$

The ψ_0 represents the initial phase of the electric field at the phase center point, and x_0 and z_0 are the x coordinate and z coordinate of the phase center. According to the orthogonality of the trigonometric function, $\cos\theta$ is multiplied on both sides of Eq.3. Then this equation is integratd from $\theta = 0$ to π to eliminate x_0 Item. Finally, the coordinate of the phase center is calculated as:

$$z_0 = \frac{c_0}{\pi^2 f}\int_0^\pi \psi(\theta)\cos\theta d\theta \tag{4}$$

Using Eq.4 to calculate in the HFSS software, the z coordinate of the antenna phase center can be obtained. The phase center coordinate of the center frequency point of each antenna can be calculated and recorded in Table 1. The largest value oscillation in the table is the z coordinate of the H antenna phase center, which is 12 mm-12.7 mm larger than the z coordinate of the other antenna phase centers. Because the loop antenna is placed at the top of the fully polarized antenna.

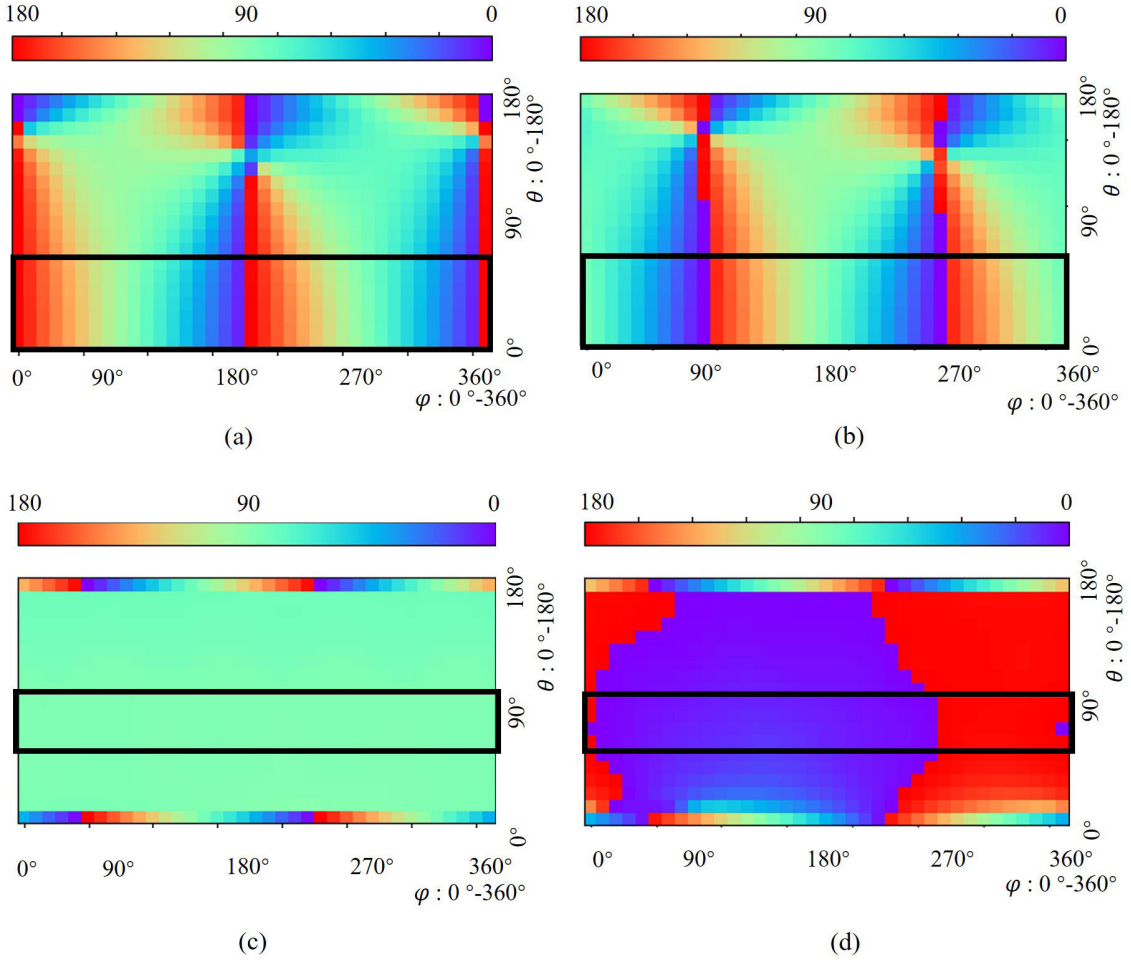

FIGURE 6. The angle of polarization ellipse long axis of each antenna in the fully polarized antenna. (a) The X antenna. (b) The Y antenna. (c) The H antenna. (d) The V antenna.

TABLE 1. The phase center of each antenna in the fully polarized antenna.

Axis	X/mm	Y/mm	Z/mm
X antenna	3.5	3.8	19.3
Y antenna	3.0	2.0	18.9
H antenna	0.1	0.1	31.6
V antenna	0.1	0.0	19.6

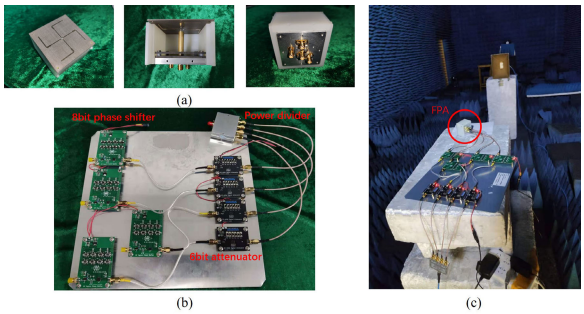

FIGURE 8. The photo of the fully polarized antenna. (a) The top view, internal structure view, and bottom view of the fully polarized antenna. (b) The control circuit of the fully polarized antenna. (c) The photo of the unknown polarized wave polarization analysis.

IV. FUNCTION VERIFICATION OF THE FULLY POLARIZED ANTENNA

In this section, the functional verification of the fully polarized antenna is present. Fig.8 (a) shows the top view, internal structure view, and bottom view of the fully polarized antenna. Fig.8 (b) shows the control circuit of the fully polarized antenna. Fig.8 (c) shows the test state of the unknown polarized wave polarization analysis. The fully polarized antenna is highlighted by a red circle named "FPA".

For a certain direction in the hemispherical airspace, two orthogonal linearly polarized antennas can be found to decompose the unknown polarized wave into orthogonal linear polarizations. The four ports of the fully polarized antenna are connected to four channels with digital phase shifters and attenuators, then connected to a power divider to form one channel. The coverage and polarization type of the fully polarized antenna can be controlled by digital phase shifters and attenuators. The power divider is connected to

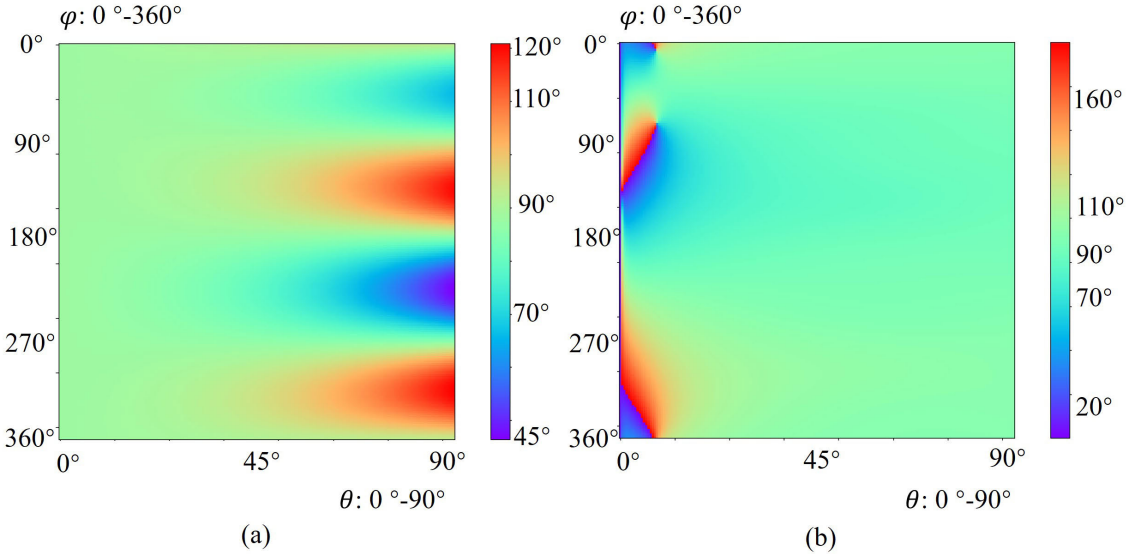

FIGURE 7. The angle difference of polarizations in the fully polarized antenna. (a) The angle difference of polarization ellipse long axis between X and Y. (b) The angle difference of polarization ellipse long axis between H and V.

the VNA port. The maximum attenuation of the attenuator is 32 dB, which can be considered as open-circuit. The unknown polarized wave comes from a horn antenna with a 25° tilt and a circularly polarized helical antenna. The experimental scene is shown in Fig.8 (c). The channel is calibrated in vertical polarization and horizontal polarization.

When the fully polarized antenna points to $\theta = 0°$, X antenna and Y antenna are adopted. When the standard horn is placed in the vertical polarization state, the Y antenna received signal amplitude is -34.6 dB and the phase is $-40.8°$; When the standard horn is placed in the horizontal polarization state, the X antenna received signal amplitude is -34.5 dB and the phase is $-57.9°$. When the standard horn is inclined at 25°, the amplitude of the received signal from the X antenna is -36.6 dB and the phase is 46°; The amplitude of the received signal from the Y antenna is -40.7 dB and the phase is 55.4°. The amplitude of the X port is 2.46 times the amplitude of the Y port, and the phase difference is $-12.3°$. The polarization ellipse is obtained by Eq. 1, the calculated axial ratio is 22.5 dB, and the calculated polarization angle is 21.76°.

The wave sources to be tested are a standard horn with a 25° tilt and an LHCP helix antenna with a 2.6 dB axial ratio. The fully polarized antenna is tested at $\theta = 0°$ and 90°, the corresponding test data is shown in Table.2.

According to Table. 2, it can be seen that the X antenna and Y antenna in the high latitude area and the H antenna and V antenna in the low latitude area can achieve high accuracy polarization analysis and restoration of unknown polarized waves. According to the reciprocity, the fully polarized antenna can also synthesize any polarized radiation in hemispherical airspace.

Compared with the tri-polarized antenna, the fully polarized antenna would produce overlapping space coverage. According to the analysis of the independent antenna's radiation performance, there is a common radiation area in the range of $40° < \theta < 80°$. This overlapping redundancy can be used to realize the reconstruction of the radiation pattern.

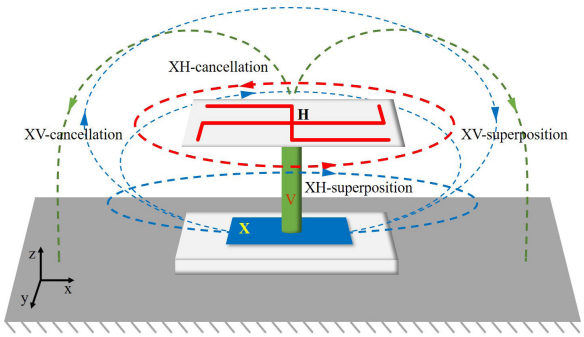

FIGURE 9. The polarization synthesis of the fully polarized antenna.

As shown in the Fig.9, the red electric field line is generated by the H antenna, the green electric field line is generated by the V antenna, and the blue electric field lines are generated by the X antenna. The X antenna and V antenna radiate vertical polarized electric field. When E field vectors of X antenna and V antenna are superposition in a direction, they cancel out in the symmetrical direction. The X antenna and H antenna radiate horizontally polarized electric fields. When E-field vectors of X antenna and H antenna are superposition in a direction, they cancel out in the symmetrical direction. The superposition and cancellation could be independently achieved in a certain direction, and would not have the same effect in the symmetrical direction.

Fig.10 shows the superposition and cancellation results of different ports at θ=55° on different planes. All data are co-pol data. When φ=0°, the polarization of θ is combined

TABLE 2. Unknown polarized wave polarization analysis.

Test condition			X-pol	Y-pol	Horn with a 25°tilt	helical antenna
θ = 0°	X port	amplitude(dB)	-34.5	\	-36.6	-56.2
		phase(°)	-57.9	\	46	-43
	Y port	amplitude(dB)	\	-34.6	-40.7	-55.3
		phase(°)	\	-40.8	55.4	-150
	AR(dB)				22.5	3.1
	polarization				LP(long axis at 21.76°)	LHCP
θ = 90°	H port	amplitude(dB)	-40.5	\	-47.7	-64.4
		phase(°)	-63.9	\	18.5	176
	V port	amplitude(dB)	\	-41.9	-43.5	-66.5
		phase(°)	\	-19.5	33.5	-61
	AR(dB)				17.8	2.4
	polarization				LP(long axis at 24.0°)	LHCP

TABLE 3. Comparison of different reported fully polarized antennas.

antennas	bandwidth(-10 dB)	coupling(dB)	fully polarized airspace
patch + monopole [5]	4.5%(-6 dB)	-24	Not mentioned
tri-monopoles [9]	3%	-18	Not mentioned
tri-slots [9]	4%	-21	Not mentioned
tri-dipole [8]	11.8%(-14 dB)	\	Not mentioned
tri-loop [10]	3.3%	-25	Not mentioned
This work	**4.1%**	**-23**	**hemisphere**

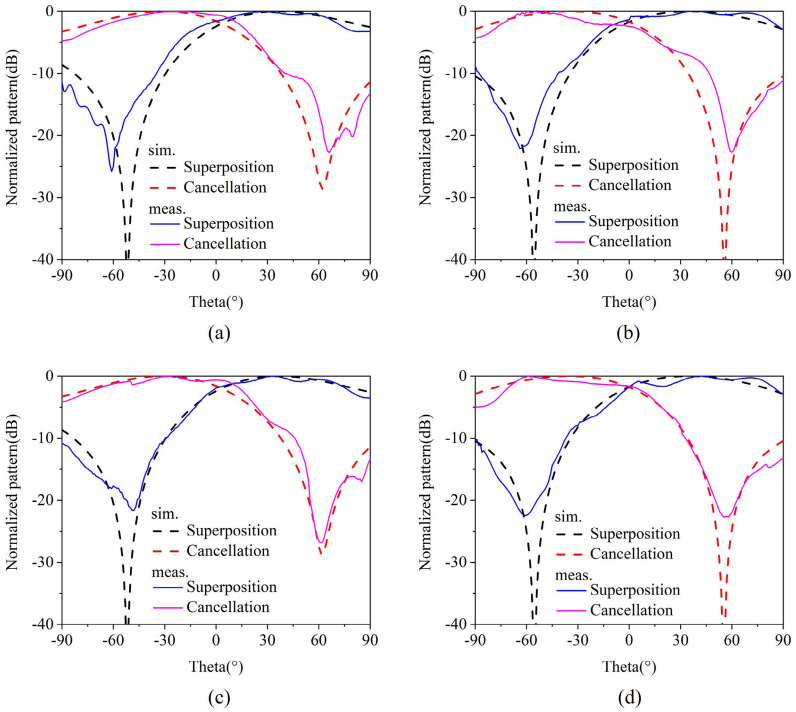

FIGURE 10. The superposition and cancellation of the same polarized ports in fully polarized antenna. (a) θ polarization superposition and cancellation between X and V.(θ=55°, φ=0°) (b) φ polarization superposition and cancellation between Y and H.(θ=55°, φ=0°) (c) θ polarization superposition and cancellation between Y and V.(θ=55°, φ=90°) (d) φ polarization superposition and cancellation between X and H.(θ=55°, φ=90°).

by X and V. And the polarization of φ is composed of Y and H, When φ=90°, the polarization of θ is a combination of Y and V. And the polarization of φ is combined by X and H.

V. CONCLUSION

In this work, a fully polarized antenna covering the hemispherical airspace has been proposed. The simulation and

measurement results verify the independent antenna radiation performance and the function of the fully polarized antenna. The orthogonality of antenna polarization is accurately verified by simulation calculation. All polarization in the hemispherical space can be covered by four ports. The experiments on the polarization analysis of unknown polarized waves and the reconstruction of antenna patterns were carried out, demonstrating the application potential of fully polarized antennas. Table.3 presents the comparison between the fully polarized antenna and other tri-polarized antennas. The fully polarized antenna proposed in this work provides an attractive candidate for applications that require accurate polarization signal detection in the hemispherical airspace. The fully polarized antenna can be widely applied in MIMO communication, full polarization detection arrays, and other applications.

REFERENCES

[1] M. R. Andrews, P. P. Mitra, and R. de Carvalho, "Tripling the capacity of wireless communications using electromagnetic polarization," *Nature*, vol. 409, no. 6818, pp. 316–318, Jan. 2001.

[2] F. Quitin, F. Bellens, A. Panahandeh, J.-M. Dricot, F. Dossin, F. Horlin, C. Oestges, and P. De Doncker, "A time-variant statistical channel model for tri-polarized antenna systems," in *Proc. 21st Annu. IEEE Int. Symp. Pers., Indoor Mobile Radio Commun.*, Sep. 2010, pp. 64–69.

[3] R. Compton, "The performance of a tripole adaptive array against cross-polarized jamming," *IEEE Trans. Antennas Propag.*, vol. AP-31, no. 4, pp. 682–685, Jul. 1983.

[4] A. Nehorai, K.-C. Ho, and B. T. G. Tan, "Minimum-noise-variance beamformer with an electromagnetic vector sensor," *IEEE Trans. Signal Process.*, vol. 47, no. 3, pp. 601–618, Mar. 1999.

[5] Z. Zhang, Y. Li, K. Wei, X. Gao, Z. Feng, and M. F. Iskander, "Three designs of polarization diversity antenna for WLAN application," in *Proc. Int. Workshop Antenna Technol. (iWAT)*, 2011, pp. 86–89.

[6] D. Gray and T. Watanabe, "Three orthogonal polarisation dra-monopole ensemble," *Electron. Lett.*, vol. 39, no. 10, pp. 766–767, 2003.

[7] N. K. Das, T. Inoue, T. Taniguchi, and Y. Karasawa, "An experiment on MIMO system having three orthogonal polarization diversity branches in multipath-rich environment," in *Proc. IEEE 60th Veh. Technol. Conf. (VTC-Fall)*, vol. 2, Sep. 2004, pp. 1528–1532.

[8] D. Psychogiou and J. Hesselbarth, "Diversity antennas for isotropic coverage," in *Proc. 3rd Eur. Wireless Technol. Conf.*, 2010, pp. 101–104.

[9] C.-Y. Chiu, J.-B. Yan, and R. D. Murch, "Compact three-port orthogonally polarized MIMO antennas," *IEEE Antennas Wireless Propag. Lett.*, vol. 6, pp. 619–622, Dec. 2007.

[10] D. Piao and Y. Wang, "Tripolarized MIMO antenna using a compact single-layer microstrip patch," *IEEE Trans. Antennas Propag.*, vol. 67, no. 3, pp. 1937–1940, Mar. 2019.

[11] *Use Ansoft HFSS to Calculate the Equivalent Phase Center of the Antenna*, Ansoft, Pittsburgh, PA, USA, 2008.

JIASHAN LIU received the B.S. degree in electronic engineering from the Beijing Institute of Technology, Beijing, China, in 2014, where he is currently pursuing the Ph.D. degree with the School of Information and Electronics.

His research interests include millimeter-wave antennas and microwave passive components.

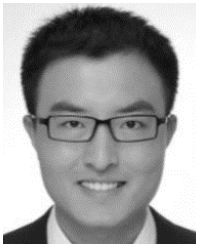

HONGDA LU (Member, IEEE) was born in Hebei, China, in 1987. He received the B.S. and Ph.D. degrees in electronic engineering from the Beijing Institute of Technology, Beijing, China, in 2010 and 2016, respectively.

He is currently working as a Postdoctoral Researcher with the Beijing Institute of Technology. His current research interests include artificial electromagnetic materials, lens antennas, millimeter-wave multibeam antennas, terahertz antennas, and terahertz phased arrays.

KE PANG was born in Henan, China, in 1995. He received the B.E. degree in electronic and information engineering from the Beijing Institute of Technology, Beijing, China, in 2018, where he is currently pursuing the master's degree.

His current research interests include millimeter-wave multiple polarized antennas and phased arrays.

ZHIPENG LIU received the B.S. degree in electromagnetic fields and microwave technology from the Beijing Institute of Technology, Beijing, China, in 2015. He is currently pursuing the Ph.D. degree with the Beijing Key Laboratory of Millimeter Wave and Terahertz Technique, Beijing.

His research interests include antenna arrays, multibeam antennas, millimeter-wave/terahertz antennas, and terahertz imaging systems.

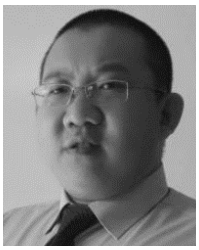

YONG LIU (Member, IEEE) was born in Heilongjiang, China, in 1977. He received the B.S. degree in physics from Jilin University, Changchun, China, in 1999, and the Ph.D. degree in electronic engineering from the Beijing Institute of Technology, Beijing, China, in 2009.

He is currently an Associate Professor with the School of Information and Electronics, Beijing Institute of Technology. His current research interests include broadband antenna, array antenna, terahertz antenna, and terahertz imaging systems.

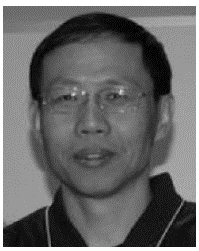

XIN LV (Member, IEEE) received the B.S., M.S., and Ph.D. degrees in electronic engineering from the Beijing Institute of Technology (BIT), in 1982, 1988, and 1993, respectively.

Since 1982, he has been with BIT, as a Lecturer, an Associate Professor, and a Professor. He currently serves as the Director of the Beijing Key Laboratory of Millimeter Wave and Terahertz Technique, BIT. His research interests include millimeter-wave and terahertz circuits, antennas, and systems.